Electrochemistry Communications 115 (2020) 106718

Contents lists available at ScienceDirect

Electrochemistry Communications

journal homepage: www.elsevier.com/locate/elecom

Group VI transition metal dichalcogenides as antifouling transducers for electrochemical oxidation of catechol-containing structures

Daniel Rojas[a,b], Flavio Della Pelle[b], Michele Del Carlo[b], Dario Compagnone[b,*], Alberto Escarpa[a,c,*]

[a] Department of Analytical Chemistry, Physical Chemistry and Chemical Engineering, Faculty of Sciences, University of Alcalá, E-28871 Alcalá de Henares, Madrid, Spain
[b] Faculty of Bioscience and Technology for Food, Agriculture and Environment, University of Teramo, 64023 Teramo, Italy
[c] Chemical Research Institute "Andres M. del Rio", University of Alcala, E-28871 Madrid, Spain

ARTICLE INFO

Keywords:
Transition metal dichalcogenides
Antifouling
Catechin
Rutin
Electrochemical transducers
Polyphenols

ABSTRACT

In this work, we present a comprehensive study comparing the electrochemical performance of MX_2 nanosheet-based electrodes (where M: Mo or W; X: S or Se). The nanosheets, obtained via a sonochemical strategy, were characterized using SEM and Raman spectroscopy to confirm the success of the exfoliation process. The electrochemical properties have been studied using a redox probe and flavonoids with an *o*-diphenol target moiety since the latter is involved in redox processes of high significance. It was revealed that selenides exhibit a better performance employing redox probes (higher k^0 and lower R_{CT}) and higher oxidation currents for oxidation of catechol-containing flavonoids (CCF). It is worthy of note that MX_2 materials also have enhanced antifouling properties toward flavonoids compared with carbon-based electrodes.

1. Introduction

Transition metal dichalcogenides (TMDs) are a family of layered compounds with the formula MX_2, where M is a transition metal element, typically from group IV to VI, and X is a chalcogen (S, Se or Te). These layers form an X-M − X structure where the atoms are strongly held together by covalent bonds, while weak Van der Waals (VdW) interactions occur between the sheets. Disruption of VdW interactions and exfoliation of the layers can be achieved by employing techniques such as electrochemistry, intercalation chemistry and liquid phase exfoliation (LPE) [1–5]. Among these techniques, LPE is the most versatile, with the ability to produce large quantities of 2D nanosheets with sizes ranging from tenths to hundreds of nanometers, and a few layers in thickness [6]. TMD nanosheets have recently attracted attention [7,8] due to their unique physical and chemical properties. In particular, these materials have been employed for detection of polyphenols, taking advantage of their physical and electronic properties [9–14]. The latter phytochemical compounds are interesting for their antioxidant properties, particularly those containing catechol moieties which present the highest antioxidant activity [15,16]. However, the electrochemical detection of these compounds is especially challenging because oxidation leads to electrode surface passivation [17]. The works reported in the literature are usually focused on a single TMD material. In contrast, in this work, a systematic study of four different Group VI TMDs is carried out for electrochemical oxidation of catechol-containing flavonoid (CCF) compounds, with the aim of clarifying the mechanism behind their antifouling properties.

2. Materials and methods

2.1. Reagents and apparatus

MoS_2, WS_2, $MoSe_2$, and WSe_2 were purchased from Alfa Aesar (Germany). Catechin, anhydrous disodium hydrogen phosphate, sodium dihydrogen phosphate hydrate, potassium ferrocyanide, potassium ferricyanide, potassium chloride, and sodium cholate were purchased from Sigma Aldrich (St Louis, MO, USA). Electrochemical measurements were carried out using an Autolab PGSTAT 12 potentiostat from Metrohm (Utrecht, Netherlands). Screen-printed electrodes (SPEs) were purchased from Dropsens S.L. (ref. DS110). Stock solutions of polyphenol standards were prepared in methanol at a concentration of 10^{-2} mol L^{-1} and stored in the dark at −20 °C.

2.2. Preparation of TMD screen-printed electrodes

Exfoliation of the TMDs was carried out from solutions containing

* Corresponding authors.
E-mail addresses: dcompagnone@unite.it (D. Compagnone), alberto.escarpa@uah.es (A. Escarpa).

https://doi.org/10.1016/j.elecom.2020.106718
Received 8 March 2020; Received in revised form 26 March 2020; Accepted 27 March 2020
Available online 29 March 2020

10 mg mL^{-1} of unexfoliated TMDs and 3 mg mL^{-1} of sodium cholate as surfactant. The solutions were first 'homogenized' in a bath sonicator (3000683 Ultrasons Selecta, Barcelona, Spain) for 15 min. Then, the solution was further sonicated in a tip sonicator for 3 h, keeping the temperature below 25 °C using an ice bath. The sonication was carried out using a pulsed program (2 s ON/ 1 s OFF and 60% amplitude) to minimize sample heating. Then, the TMD dispersion was centrifuged for 30 min at 500 g to eliminate unexfoliated material. The supernatant was collected and washed/centrifuged with water, ethanol, and isopropanol to eliminate the excess of surfactant; each washing step was repeated in triplicate. The washed TMDs were kept dry for further use. Electrode modification was carried out by drop-casting 5 μL of a 1 mg mL^{-1} dispersion of the washed TMDs

2.3. Electrochemical characterization

The SPE-TMDs were investigated using cyclic voltammetry (CV) and electrochemical impedance spectroscopy (EIS) carried out in 5 mmol L^{-1} $[Fe(CN)_6]^{3-/4}$. EIS experiments were performed using a sinusoidal wave of amplitude 10 mV in the 10^5 to 10^{-2} Hz frequency range at open circuit potential.

2.4. Microstructure and elemental characterization

Raman spectra were recorded using an Alpha 300 AR (WITec, Ulm, Germany) confocal Raman microscope with laser wavelength set at 532 nm. Scanning electron microscopy (SEM) micrographs were obtained with a JEOL 6335F microscope (JEOL USA, Massachusetts, United States) using an acceleration voltage of 5 kV. The size distribution of the TMD flakes (assessed on an average number of 50–100 'particles') was evaluated with ImageJ, v.1.49.p; the micrographs were converted into binary images by setting a threshold and then analyzed [18].

3. Results and discussion

There is a lack of systematic studies about the electrocatalytic properties of TMDs, in particular towards polyphenols. Motivated by the high performance previously obtained in our group for MoS_2 [20,21], the electrocatalytic properties of group VI MX_2 (MoS_2, WS_2, $MoSe_2$, and WSe_2) towards CCF have been systematically evaluated in this work.

3.1. Exfoliation and characterization of MX_2 nanosheets

LPE in water/sodium cholate solutions was chosen for the production of the MX_2 nanosheets. This approach has been previously reported to achieve a comparable degree of exfoliation for the different TMDs [19], which is difficult when employing organic solvents or other water/surfactant mixtures [20].

To confirm the exfoliation process, scanning electron microscopy (SEM) and Raman spectroscopy were performed. SEM images of the bulk and exfoliated MX_2 are presented in Fig. 1. In all cases, the lateral size was greatly reduced compared to the bulk material, confirming the formation of MX_2 nanosheets. The size distribution of the exfoliated materials is shown in Fig. S1. The mean size was 193 ± 94, 170 ± 33, 173 ± 26 and 164 ± 54 for MoS_2, WS_2, $MoSe_2$ and WSe_2, respectively. Furthermore, the nanosheets show a rough surface and wrinkled edges compared to the smooth surface and defined edges of the bulk material that have presumably been incorporated during the exfoliation process [21].

Raman spectroscopy was employed to further characterize the nanosheets as it is useful for studying the layer thickness and crystalline structure. Fig. 2 shows the Raman spectra of bulk and exfoliated MX_2. The MoS_2 spectra consists of two different bands, the in-plane (E^1_{2g}) and out-of-plane (A_{1g}) vibration modes at around 380 and 405 cm^{-1}, respectively. Considering the data from the exfoliated material, softening and broadening (FWHM increase ~ 2 cm^{-1}) of both vibration modes are observed with respect to the bulk material. The $MoSe_2$ spectra show a well-defined peak at 250 cm^{-1} attributed to the A_{1g} vibration mode. In the case of the exfoliated material, as in MoS_2, the peak is slightly softened and notably broadened (FWHM from 9 to 17 cm^{-1}) compared to the bulk material. These results indicate a decrease in the number of layers and lateral size, suggesting that the exfoliation process was successful [21,22]. In the case of WS_2, two peaks are recorded at 350 cm^{-1} and 420 cm^{-1}, ascribed to E^1_{2g} and A_{1g}, respectively. In this case no significant softening or broadening is observed. However, the ratio between the intensity of the peaks E^1_{2g} and A_{1g} is higher in the case of the exfoliated material (1.7 vs. 1); this is also considered characteristic of a successful exfoliation [23,24]. WSe_2 presents E^1_{2g} and A_{1g} modes overlapping and centered around 250 cm^{-1}. The Raman shift difference between E^1_{2g} and A_{1g} peaks is related to the thickness and varies from 3 cm^{-1} to 11 cm^{-1} from bulk to monolayer, respectively [25]. In the recorded spectra, a shoulder peak becomes more distinguishable in the case of the exfoliated material, indicating a higher separation of the vibration modes and hence a successful exfoliation. In order to further confirm the chemical composition of the sheets, the presence of MoO_3 (820 cm^{-1}) and WO_3 (697 cm^{-1}) vibrational modes have also been studied. In Fig. S2, no peaks related to the oxides can be seen, except in the case of WS_2, where a slight signal can be seen at 698 cm^{-1}. A signal of lower intensity is present in the spectrum of the exfoliated material, which can be attributed to the elimination of the oxides during the washing steps [26].

3.2. Electrochemical characterization

Electrode kinetics is a critical aspect in the development of new nanomaterials for sensing purposes. In particular, fast kinetics are desirable for application as an electrochemical transducer for molecules of interest. Firstly, the possible influence of the surfactant was evaluated by cyclic voltammetry (CV) in a phosphate buffer, recording the inherent electrochemistry of these materials (Fig. S3). It can be seen that the anodic peak due to the oxidation of the metallic center of the MX_2 become more evident and sharper and a new cathodic peak appeared due to the oxygen reduction reaction (ORR) on the washed samples in comparison with the just exfoliated ones. These results suggest that despite the great influence of the surfactant, the washing steps made it possible to obtain well-defined voltammograms due to the inherent electrochemistry of the TMDs, comparable to those reported in literature which employ exfoliation methods without using surfactant [27,28]. Electrochemical characterization of the selected Group VI MX_2 compounds was then carried out via CV and electrochemical impedance spectroscopy (EIS), using $[Fe(CN)_6]^{3-/4-}$ as an inner-sphere redox probe. In each technique, the heterogeneous electron transfer rate (k^0) is inversely proportional to the peak separation (ΔE_p) and the resistance to charge transfer (R_{CT}), respectively. In fact, k^0 can be estimated from the ΔE_p obtained at different scan rates using the Nicholson method [29]. Fig. 3A shows the CVs obtained using different MX_2 modified electrodes. As can be seen from Fig. 3B the ΔE_p values follow the trend: MoS_2 (275 ± 19 mV) > WS_2 (203 ± 13 mV) > WSe_2 (190 ± 18 mV) > $MoSe_2$ (150 ± 10 mV), showing the superior electrochemical performance of the selenides versus the sulfides. Applying the Nicholson method in the 5 to 100 mV/s scan rate range, k^0 values of $[(3.7 \pm 0.4) < (5.5 \pm 0.4) < (6.4 \pm 0.5) < (7.8 \pm 0.7)]\cdot 10^{-4}$ cm s^{-1} are obtained for MoS_2, WS_2, WSe_2, and $MoSe_2$, respectively. EIS experiments were also carried out and the data were displayed as Nyquist plots, where the diameter of the semicircle corresponds to the charge-transfer resistance value and the linear part to the diffusion-controlled region. The impedance data were successfully fitted using the Randles equivalent circuit ($\chi^2 < 0.025$) shown in the inset of Fig. 3C, where R_s, R_{CT}, C_{DL}, and Z_W represent the solution resistance, charge-transfer resistance, double-layer capacitance and Warburg impedance, respectively. Fig. 3C shows the impedance data obtained for each electrode. In the range of frequencies

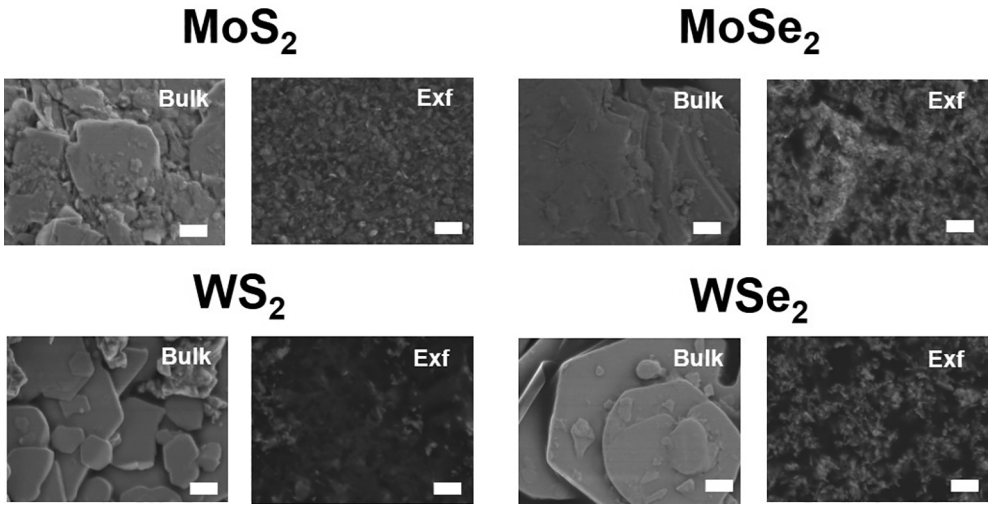

Fig. 1. Scanning electron micrographs of bulk and exfoliated MX_2. Scale bar: 1 μm.

studied, mixed kinetic and diffusion control of the reaction is observed. By fitting the experimental data to the Randles equivalent circuit R_{CT} data can be extracted as follows: 1170 ± 50 Ω, 954 ± 96 Ω, 727 ± 115 Ω and 431 ± 75 Ω for MoS_2, WS_2, WSe_2, and $MoSe_2$. The trend in R_{CT} values (see Fig. 3D) was thus identical to the trend in ΔE_p. These data are also in agreement with the previously reported electrical conductivity of thin-film networks of MX_2 (WSe_2 > $MoSe_2$ > WS_2 > MoS_2) [30].

3.3. Electrochemical response towards CCF oxidation

The study of the electrochemical behaviour of MX_2 was extended to CCF oxidation, taking catechin and rutin as representative of flavonoid and glycosylated flavonoid compounds, respectively. As can be seen from Fig. 4A, superior electrochemical response towards catechin and rutin followed the same order for both CCFs (WSe_2 > $MoSe_2$ > WS_2 > MoS_2), exhibiting a quasi-reversible process.

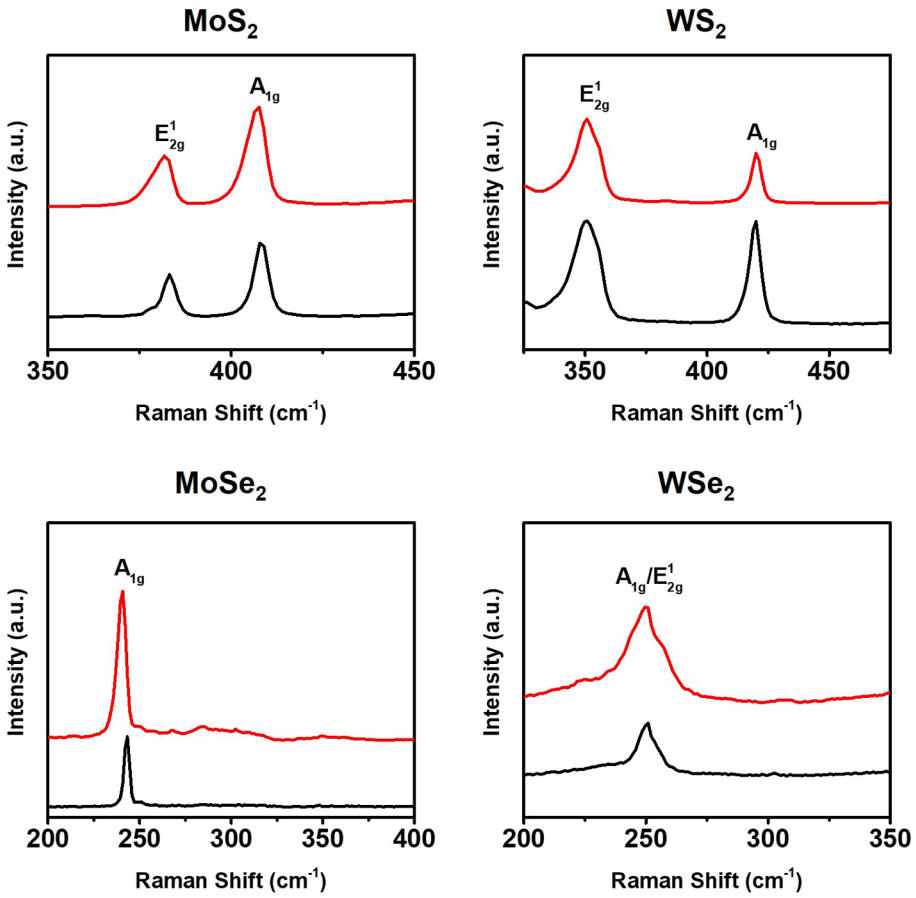

Fig. 2. Raman spectra of exfoliated (red) and bulk (black) MX_2. (For interpretation of the references to color in this figure legend, the reader is referred to the web version of this article.)

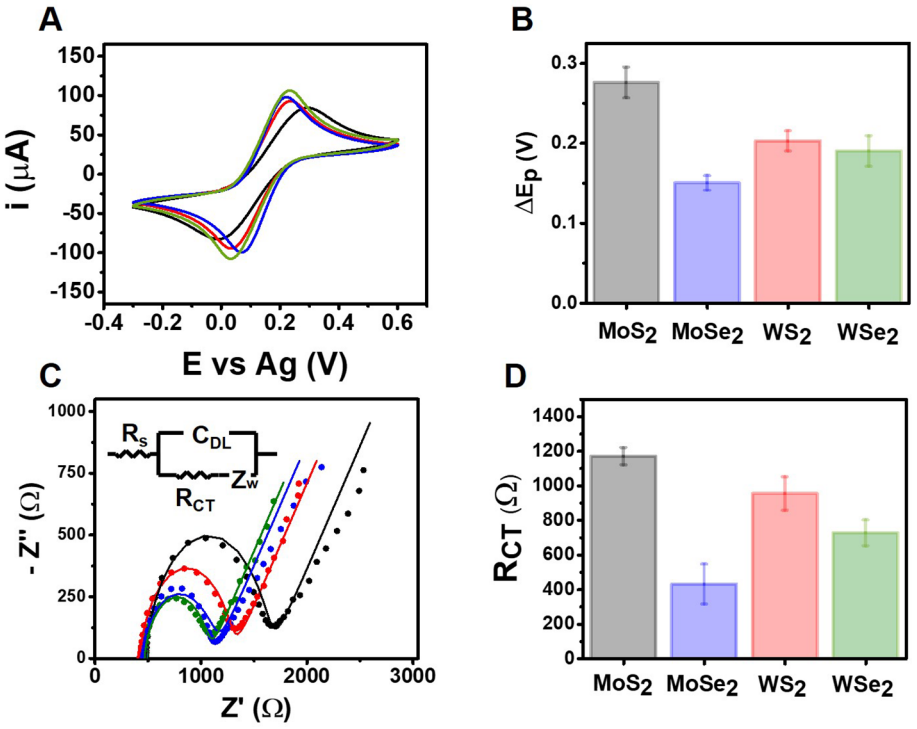

Fig. 3. MX_2 electrochemical characterization (A) CV performed at 50 mV s^{-1}, (B) ΔE_p data extracted from CV (C) EIS spectra (D) R_{CT} data extracted from spectra. Electrochemical characterization employing 5 mM $[Fe(CN)_6]^{3-/4-}$ in 0.1 M KCl as redox probe Data taken from 5 different electrodes. Color code is maintained for each material in all panels.

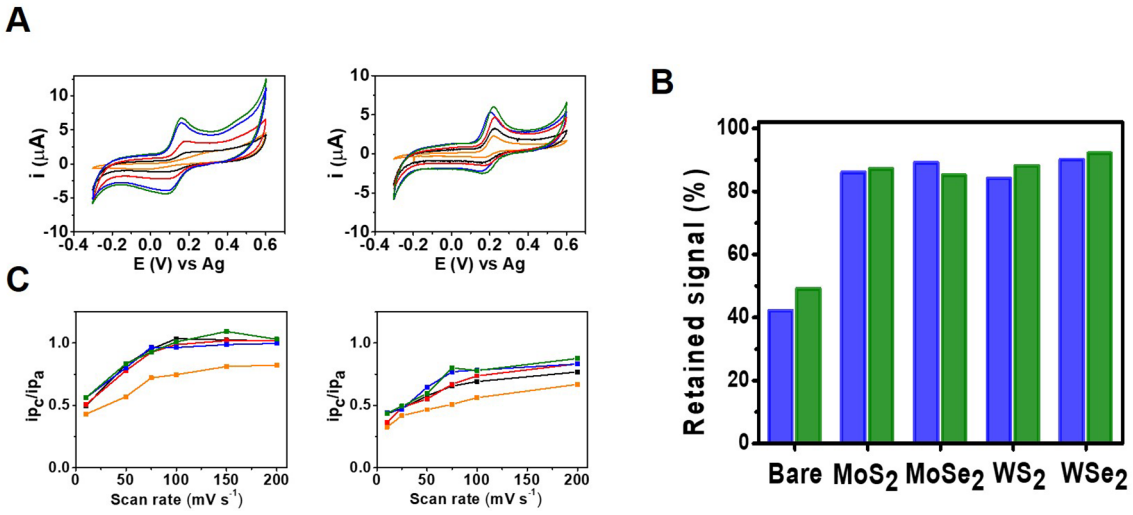

Fig. 4. A) Cyclic voltammograms of 0.1 mM Catechin and Rutin on bare and MX_2 modified electrodes recorded at 25 mV s^{-1} at pH = 7. B) Retained signal after 10 measurements employing MX_2-based electrodes for catechin (blue) and rutin (green). Bare electrode was added for comparison. C) Plot of the ip_a/ip_c ratio for each electrode obtained at different scan rates for Catechin and Rutin. Bare electrode (black) MoS2 (blue), WS2 (red), MoSe2 (blue) and WSe2 (green). (For interpretation of the references to color in this figure legend, the reader is referred to the web version of this article.)

This result shows the different electroactivities of the various MX_2 compounds, which in all cases represented a significant improvement (in terms of decreasing ΔE_p and increasing ip_a) compared to the carbon-based screen-printed electrode. It is also worth noting that the peak intensities corresponding to flavonoid oxidation are consistent with the intrinsic conductivity and electrochemical performance obtained with $[Fe(CN)_6]^{3-/4-}$. The fouling effect of catechin and rutin was also evaluated and the results are shown in Fig. 4B. The fouling resistance is increased in all TMDs compared with the bare carbon-based, screen-printed electrode, as already reported by our group for MoS_2 [31,32].

On top of that, as shown in Fig. 4C, the ratio between the cathodic and anodic peaks differs between the TMDs and the bare electrode. If we compare the data acquired at the same scan rate, the ratio ip_c/ip_a is higher for MX_2 than for the carbon-based, screen-printed electrode. As the scan rate is increased, the ip_c/ip_a ratio increases, indicating an electrochemical-chemical mechanism (EC), in which an electrochemical reaction step (E) is followed by a coupled chemical reaction (C) [33]. CCFs have been reported to follow this type of mechanism on glassy carbon electrodes, with the formation of a phenoxy radical intermediate [34]. The electrogenerated products in this reaction, CCF oligomers and polymers, have been shown to be able to block the electrode surface, causing so-called electrode fouling [35–38]. In fact, we observed notable electrode fouling in our experiments employing carbon-based screen-printed electrodes. Interestingly, this phenomenon is not observed on MX_2-based electrodes. An explanation for this observation is proposed, based on the obtained results. Scheme 1 shows the proposed reaction scheme. Once the phenoxy radical (R) has been electrogenerated it can follow two reaction pathways: (i)

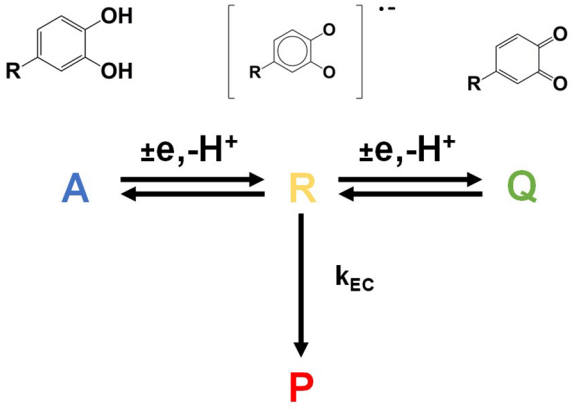

Scheme 1. Proposed reaction scheme of CCF oxidation on MX_2-based electrodes.

electrochemical oxidation to the quinone (Q) derivative of the corresponding CCF, or (ii) chemical reaction with the corresponding CCF polymer/oligomer (P) capable of blocking the electrode surface. It can be inferred from the ip_c/ip_a values that the formation of Q is favored over P with MX_2-based electrodes since ip_c/ip_a tends to 1, all R produced is converted to Q, which is detected in the reverse scan. On the other hand, ip_c/ip_a is lower for carbon-based electrodes than for MX_2 at all scan rates studied, suggesting that less Q is formed. The fouling effect is much higher in the case of carbon-based screen-printed electrodes, which further indicates the preferential formation of P compared to MX_2-based electrodes. These results suggest that MX_2 compounds are able to preferentially drive the radical intermediate evolution towards the quinone product, avoiding polymerization of polyphenols on the electrode surface and the subsequent fouling effect.

4. Conclusions

In our study of MX_2 nanosheet-based electrodes, successfully exfoliated selenides showed superior electrochemical performance to the corresponding sulfides with higher k^0, lower R_{CT} and higher electrocatalytic oxidation of CCF, following the order: $WSe_2 > MoSe_2 > WS_2 > MoS_2$. A dramatic improvement in the antifouling properties was shown by MX_2-based nanosheets compared to carbon-based electrodes, revealing the key role of these materials. This behavior can be explained by an EC mechanism in which MX_2 preferentially drives the oxidation of CCF towards the quinone product, avoiding polymerization of the polyphenols and the subsequent fouling effect. These findings confirm the outstanding antifouling properties of TMDs towards polyphenols and give an experimentally supported explanation of these antifouling properties. These results pave the way for a high-performance electrochemical analysis TMD for use with non-ideal samples.

Declaration of Competing Interest

The authors declare that they have no known competing financial interests or personal relationships that could have appeared to influence the work reported in this paper.

Acknowledgments

DR, MDC, and AE acknowledge the European Union's Horizon 2020 research and innovation program under the Marie Skłodowska-Curie (grant agreement 713714) and co-funding of University of Teramo and Abruzzo region.

FDP acknowledges the Ministry of Education, University and Research (MIUR) and European Social Fund (ESF) for the PON R&I 2014-2020 program, action 1.2 'AIM: Attraction and International Mobility' (AIM1894039-3).

MDC acknowledges the Fund FARDIB 2019, Project: NUOVI MATERIALI, BIOLOGICI E SINTETICI, PER APPLICAZIONI ANALITICHE NEL CAMPO DEGLI ALIMENTI, University of Teramo, Italy.

DC acknowledges the PRIN 2017 ACTUaL project of the Italian Ministry of Education, University and Research (MIUR) for funding.

AE acknowledges Spanish Ministry of Economy, Industry and Competitiveness (CTQ2017-86441-C2-1-R) and TRANSNANOAVANSENS program (S2018/NMT-4349) from the Community of Madrid.

Appendix A. Supplementary data

Supplementary data to this article can be found online at https://doi.org/10.1016/j.elecom.2020.106718.

References

[1] X. Cai, Y. Luo, B. Liu, H.-M. Cheng, Preparation of 2D material dispersions and their applications, Chem. Soc. Rev. 47 (2018) 6224–6266, https://doi.org/10.1039/C8CS00254A.

[2] W. Choi, N. Choudhary, G.H. Han, J. Park, D. Akinwande, Y.H. Lee, Recent development of two–dimensional transition metal dichalcogenides and their applications, Mater. Today 20 (2017) 116–130, https://doi.org/10.1016/j.mattod.2016.10.002.

[3] C. Backes, T.M. Higgins, A. Kelly, C. Boland, A. Harvey, D. Hanlon, J.N. Coleman, Guidelines for exfoliation, characterization and processing of layered materials produced by liquid exfoliation, Chem. Mater. 29 (2017) 243–255, https://doi.org/10.1021/acs.chemmater.6b03335.

[4] X. Chia, M. Pumera, Layered transition metal dichalcogenide electrochemistry: journey across the periodic table, Chem. Soc. Rev. 47 (2018) 5602–5613, https://doi.org/10.1039/C7CS00846E.

[5] A. Ambrosi, M. Pumera, Exfoliation of layered materials using electrochemistry, Chem. Soc. Rev. 47 (2018) 7213–7224, https://doi.org/10.1039/C7CS00811B.

[6] X. Zhang, Z. Lai, C. Tan, H. Zhang, Solution-processed two-dimensional MoS_2 nanosheets: Preparation, hybridization, and applications, Angew. Chemie Int. Ed. 55 (2016) 8816–8838, https://doi.org/10.1002/anie.201509933.

[7] A.T.E. Vilian, B. Dinesh, S.-M. Kang, U.M. Krishnan, Y.S. Huh, Y.-K. Han, Recent advances in molybdenum disulfide-based electrode materials for electroanalytical applications, Microchim. Acta 186 (2019) 203, https://doi.org/10.1007/s00604-019-3287-y.

[8] A. Sinha, B. Dhanjai, Y. Tan, H. Huang, X. Zhao, J. Dang, R. Chen, Jain, MoS2 nanostructures for electrochemical sensing of multidisciplinary targets: A review, TrAC Trends Anal. Chem. 102 (2018) 75–90, https://doi.org/10.1016/J.TRAC.2018.01.008.

[9] W. Zhang, L. Zong, G. Geng, Y. Li, Y. Zhang, Enhancing determination of quercetin in honey samples through electrochemical sensors based on highly porous polypyrrole coupled with nanohybrid modified GCE, Sensors Actuators B Chem. 257 (2018) 1099–1109, https://doi.org/10.1016/J.SNB.2017.11.059.

[10] B. Xu, B. Zhang, L. Yang, F. Zhao, B. Zeng, Electrochemical determination of luteolin using molecularly imprinted poly-carbazole on MoS2/graphene-carbon nanotubes nanocomposite modified electrode, Electrochim. Acta 258 (2017) 1413–1420, https://doi.org/10.1016/j.electacta.2017.12.004.

[11] Y. Zhang, Z. Liu, L. Zou, B. Ye, A new voltammetry sensor platform for eriocitrin based on CoS2-MoS2-PDDA-GR nanocomposite, Talanta 189 (2018) 345–352, https://doi.org/10.1016/J.TALANTA.2018.07.004.

[12] B. Xu, L. Yang, F. Zhao, B. Zeng, A novel electrochemical quercetin sensor based on Pd/MoS2-ionic liquid functionalized ordered mesoporous carbon, Electrochim. Acta 247 (2017) 657–665, https://doi.org/10.1016/J.ELECTACTA.2017.06.130.

[13] H. Zhang, T. Wang, Y. Qiu, F. Fu, Y. Yu, Electrochemical behavior and determination of baicalin on a glassy carbon electrode modified with molybdenum disulfide nano-sheets, J. Electroanal. Chem. 775 (2016) 286–291, https://doi.org/10.1016/J.JELECHEM.2016.06.017.

[14] S. Su, W. Cao, C. Zhang, X. Han, H. Yu, D. Zhu, J. Chao, C. Fan, L. Wang, Improving performance of MoS_2-based electrochemical sensors by decorating noble metallic nanoparticles on the surface of MoS_2 nanosheet, RSC Adv. 6 (2016) 76614–76620, https://doi.org/10.1039/C6RA12401A.

[15] F. Della Pelle, A. Scroccarello, M. Sergi, M. Mascini, M. Del Carlo, D. Compagnone, Simple and rapid silver nanoparticles based antioxidant capacity assays: Reactivity study for phenolic compounds, Food Chem. 256 (2018), https://doi.org/10.1016/j.foodchem.2018.02.141.

[16] J.M. Brcanović, A.N. Pavlović, S.S. Mitić, G.S. Stojanović, D.D. Manojlović, B.M. Kaličanin, J.N. Veljković, J.N. Veljkovi, S.S.M. Jelena, M. Brcanovi, Aleksandra N. Pavlovi, G.S. Stojanovi, D.D. Manojlovi, B.M. Kalianin, Cyclic voltammetry determination of antioxidant capacity of cocoa powder, dark chocolate and milk chocolate samples: Correlation with spectrophotometric assays and individual phenolic compounds, Food Technol. Biotechnol. 51 (2013) 460–470, https://doi.org/10.1097/BTE.0000000000000074.

[17] X. Yang, J. Kirsch, J. Fergus, A. Simonian, Modeling analysis of electrode fouling during electrolysis of phenolic compounds, Electrochim. Acta 94 (2013) 259–268, https://doi.org/10.1016/j.electacta.2013.01.019.
[18] C.A. Schneider, W.S. Rasband, K.W. Eliceiri, NIH Image to ImageJ: 25 years of image analysis, Nat. Methods. 9 (2012) 671–675, https://doi.org/10.1038/nmeth.2089.
[19] C. Backes, B.M. Szydłowska, A. Harvey, S. Yuan, V. Vega-Mayoral, B.R. Davies, P. Zhao, D. Hanlon, E.J.G. Santos, M.I. Katsnelson, W.J. Blau, C. Gadermaier, J.N. Coleman, Production of highly monolayer enriched dispersions of liquid-exfoliated nanosheets by liquid cascade centrifugation, ACS Nano 10 (2016) 1589–1601, https://doi.org/10.1021/acsnano.5b07228.
[20] E.D. Grayfer, M.N. Kozlova, V.E. Fedorov, Colloidal 2D nanosheets of MoS_2 and other transition metal dichalcogenides through liquid-phase exfoliation, Adv. Colloid Interface Sci. 245 (2017) 40–61, https://doi.org/10.1016/J.CIS.2017.04.014.
[21] A. Sajedi-Moghaddam, C.C. Mayorga-Martinez, E. Saievar-Iranizad, Z. Sofer, M. Pumera, Exfoliated transition metal dichalcogenide (MX_2; M = Mo, W; X = S, Se, Te) nanosheets and their composites with polyaniline nanofibers for electrochemical capacitors, Appl. Mater. Today 16 (2019) 280–289, https://doi.org/10.1016/J.APMT.2019.06.002.
[22] H.S.S. Ramakrishna Matte, A. Gomathi, A.K. Manna, D.J. Late, R. Datta, S.K. Pati, C.N.R. Rao, MoS2 and WS2 analogues of graphene, Angew. Chemie Int. Ed. 49 (2010) 4059–4062, https://doi.org/10.1002/anie.201000009.
[23] A. Berkdemir, H.R. Gutiérrez, A.R. Botello-Méndez, N. Perea-López, A.L. Elías, C.I. Chia, B. Wang, V.H. Crespi, F. López-Urías, J.C. Charlier, H. Terrones, M. Terrones, Identification of individual and few layers of WS_2 using Raman spectroscopy, Sci. Rep. 3 (2013), https://doi.org/10.1038/srep01755.
[24] E. Rahmanian, C.C. Mayorga-Martinez, R. Malekfar, J. Luxa, Z. Sofer, M. Pumera, 1T-Phase tungsten chalcogenides (WS_2, WSe_2, WTe_2) decorated with TiO2 nanoplatelets with enhanced electron transfer activity for biosensing applications, ACS Appl. Nano Mater. 1 (2018) 7006–7015, https://doi.org/10.1021/acsanm.8b01796.
[25] H. Sahin, S. Tongay, S. Horzum, W. Fan, J. Zhou, J. Li, J. Wu, F.M. Peeters, Anomalous Raman spectra and thickness-dependent electronic properties of WSe_2, Phys. Rev. B - Condens. Matter Mater. Phys. 87 (2013) 165409, https://doi.org/10.1103/PhysRevB.87.165409.
[26] Z. Gholamvand, D. McAteer, C. Backes, N. McEvoy, A. Harvey, N.C. Berner, D. Hanlon, C. Bradley, I. Godwin, A. Rovetta, M.E.G. Lyons, G.S. Duesberg, J.N. Coleman, Comparison of liquid exfoliated transition metal dichalcogenides reveals $MoSe_2$ to be the most effective hydrogen evolution catalyst, Nanoscale 8 (2016) 5737–5749, https://doi.org/10.1039/C5NR08553E.
[27] M. Zafir Mohamad Nasir, Z. Sofer, M. Pumera, Effect of electrolyte pH on the inherent electrochemistry of layered transition-metal dichalcogenides (MoS2, MoSe2, WS2, WSe2), ChemElectroChem 2 (2015) 1713-1718. doi:10.1002/celc.201500259.
[28] S.M. Tan, Z. Sofer, J. Luxa, M. Pumera, Aromatic-exfoliated transition metal dichalcogenides: implications for inherent electrochemistry and hydrogen evolution, ACS Catal. 6 (2016) 4594–4607, https://doi.org/10.1021/acscatal.6b00761.
[29] R.S. Nicholson, Theory and application of cyclic voltammetry for measurement of electrode reaction kinetics, Anal. Chem. 37 (1965) 1351–1355, https://doi.org/10.1021/ac60230a016.
[30] G. Cunningham, D. Hanlon, N. McEvoy, G.S. Duesberg, J.N. Coleman, Large variations in both dark- and photoconductivity in nanosheet networks as nanomaterial is varied from MoS_2 to WTe_2, Nanoscale 7 (2015) 198–208, https://doi.org/10.1039/C4NR04951A.
[31] D. Rojas, F. Della Pelle, E. Del Carlo, D. Michele Fratini, Alberto Compagnone Escarpa, M. Del Carlo, E. Fratini, A. Escarpa, D. Compagnone, Nanohybrid carbon black-molybdenum disulfide transducers for preconcentration-free voltammetric detection of the olive oil o-diphenols hydroxytyrosol and oleuropein, Microchim. Acta 186 (2019) 363, https://doi.org/10.1007/s00604-019-3418-5.
[32] F. Della Pelle, D. Rojas, A. Scroccarello, M. Del Carlo, G. Ferraro, C. Di Mattia, M. Martuscelli, A. Escarpa, D. Compagnone, High-performance carbon black/molybdenum disulfide nanohybrid sensor for cocoa catechins determination using an extraction-free approach, Sensors Actuators B Chem. 296 (2019) 126651, https://doi.org/10.1016/j.snb.2019.126651.
[33] C. Sandford, M.A. Edwards, K.J. Klunder, D.P. Hickey, M. Li, K. Barman, M.S. Sigman, H.S. White, S.D. Minteer, A synthetic chemist's guide to electroanalytical tools for studying reaction mechanisms, Chem. Sci. 10 (2019) 6404–6422, https://doi.org/10.1039/c9sc01545k.
[34] H.P. Hendrickson, A.D. Kaufman, C.E. Lunte, Electrochemistry of catechol-containing flavonoids, J. Pharm. Biomed. Anal. 12 (1994) 325–334, https://doi.org/10.1016/0731-7085(94)90007-8.
[35] M. Polášek, I. Petriška, M. Pospíšilová, L. Jahodář, Use of molybdate as novel complex-forming selector in the analysis of polyhydric phenols by capillary zone electrophoresis, Talanta 69 (2006) 192–198, https://doi.org/10.1016/J.TALANTA.2005.09.026.
[36] M. DelCarlo, A. Amine, M. Haddam, F. DellaPelle, G.C. Fusella, D. Compagnone, Selective voltammetric analysis of o-diphenols from olive oil using Na_2MoO_4 as electrochemical mediator, Electroanalysis 24 (2012) 889–896, https://doi.org/10.1002/elan.201100603.
[37] M.-E. Ghica, A. Brett, Electrochemical oxidation of rutin, Electroanalysis 17 (2005) 313–318, https://doi.org/10.1002/elan.200403100.
[38] P. Janeiro, A.M. Oliveira Brett, Catechin electrochemical oxidation mechanisms, Anal. Chim. Acta 518 (2004) 109–115, https://doi.org/10.1016/j.aca.2004.05.038.